International Journal of Nanomedicine

Dovepress
open access to scientific and medical research

Open Access Full Text Article

ORIGINAL RESEARCH

Chemodynamic PtMn Nanocubes for Effective Photothermal ROS Storm a Key Anti-Tumor Therapy in-vivo

Chen Wang[1,*], Hongmei Zhou[1,*], Mekhrdod S Kurboniyon[2], Yanping Tang[1], Zhengmin Cai[1], Shufang Ning[1], Litu Zhang[1], Xinqiang Liang[1]

[1]Department of Research & Guangxi Cancer Molecular Medicine Engineering Research Center & Guangxi Key Laboratory of Basic and Translational Research for Colorectal Cancer, Guangxi Medical University Cancer Hospital, Nanning, People's Republic of China; [2]National Academy of Sciences of Tajikistan, Dushanbe, Tajikistan

*These authors contributed equally to this work

Correspondence: Litu Zhang; Xinqiang Liang, Department of Research and Guangxi Cancer Molecular Medicine Engineering Research Center and Guangxi Key Laboratory of Basic and Translational Research for Colorectal Cancer, Guangxi Medical University Cancer Hospital, Nanning, People's Republic of China, Email zhanglitu@gmail.com; xx03716@163.com

Background: Chemodynamic therapy (CDT) is a new treatment approach that is triggered by endogenous stimuli in specific intracellular conditions for generating hydroxyl radicals. However, the efficiency of CDT is severely limited by Fenton reaction agents and harsh reaction conditions.

Methods: Bimetallic PtMn nanocubes were rationally designed and simply synthesized through a one-step high-temperature pyrolysis process by controlling both the nucleation process and the subsequent crystal growth stage. The polyethylene glycol was modified to enhance biocompatibility.

Results: Benefiting from the alloying of Pt nanocubes with Mn doping, the structure of the electron cloud has changed, resulting in different degrees of the shift in electron binding energy, resulting in the increasing of Fenton reaction activity. The PtMn nanocubes could catalyze endogenous hydrogen peroxide to toxic hydroxyl radicals in mild acid. Meanwhile, the intrinsic glutathione (GSH) depletion activity of PtMn nanocubes consumed GSH with the assistance of Mn^{3+}/Mn^{2+}. Upon 808 nm laser irradiation, mild temperature due to the surface plasmon resonance effect of Pt metal can also enhance the Fenton reaction.

Conclusion: PtMn nanocubes can not only destroy the antioxidant system via efficient reactive oxygen species generation and continuous GSH consumption but also propose the photothermal effect of noble metal for enhanced Fenton reaction activity.

Keywords: noble metal, Mn-doping, Fenton reaction, photothermal effect, chemodynamic therapy

Introduction

Cancer, also known as malignant tumors, is still a fatal disease that threatens human health around the world.[1–3] Compared with early stage tumors, the treatment of malignant tumors faces many difficulties, such as not easy to cure, easy to recur and metastasis, causing necrosis, bleeding, co-infection, and other complications. In severe cases, it can easily lead to organ failure and death.[4–7] Currently, the main clinical treatment methods are still surgery, chemotherapy, and radiotherapy. However, traditional treatment methods cannot completely cure cancer, but only prolong the survival time of patients.[4,8–10] The treatment process not only causes great pain to patients but also costs a lot of money, manpower, and material resources. Significantly, with the continuous development of nanotechnology, more and more nanomaterials are being applied to cancer research.[11–19] Using nanomaterials as carriers, biomaterials with specific structure and function can be designed and engineered specifically for tumor cells, the tumor microenvironment (TME), and the immune system to overcome toxicity and improve drug capacity and bioavailability.[20–28] Thus, the development

Received: 25 January 2024
Accepted: 21 May 2024
Published: 30 May 2024

of effective and safe cancer treatments has become a hot research topic. These include phototherapy, sonodynamic therapy, chemodynamic therapy (CDT), immunotherapy, gene therapy, and gas therapy.[29–32]

CDT is a new therapeutic approach that is triggered by endogenous chemical conditions in the TME.[33–35] Due to the acidic condition and overexpression of hydrogen peroxide (H_2O_2), nanomaterials can generate more cytotoxic hydroxyl radicals (·OH) through Fenton/Fenton-like reaction, resulting in irreversible damage to biological macromolecules.[26,36,37] CDT is considered a promising strategy for tumor therapy and is gaining attention due to its significant advantages such as high tumor specificity, good selectivity, and low systemic side effects.[38–42] The optimal pH reaction condition of the Fenton reaction is 3~4. In addition, the overexpression of antioxidants (such as glutathione, GSH) is also the main characteristic of the intracellular environment.[43–46] High-valence metal ions can deplete GSH and transform into low-valence states, while through Fenton/Fenton-like reaction, low-valence metal ions can also generate ·OH in proportion to H_2O_2, achieving the therapeutic effect of CDT.[47] Therefore, to achieve good CDT efficacy, it is important to enhance the Fenton reaction efficiency, such as increasing the activity of Fenton reaction reagents, increasing the content of H_2O_2 inside the tumor, reducing the consumption of reactive oxygen species (ROS) and regulating the pH value of the TME.[48] In particular, the multivalent Mn ions are responsive to the TME and can be released. Mn^{2+} reacts with the abundant intracellular H_2O_2 to produce ·OH. Therefore, multivalent Mn ions can maximize the efficacy of CDT and increase the efficiency of the Fenton reaction, which has been shown to enhance CDT therapy in cancer.[49,50]

The combination of CDT and other treatment methods has become an inevitable trend compared to single-model therapy. The excellent light, ultrasonic, and magnetic stimulation response characteristics of nanomaterials make it possible to combine CDT with chemotherapy, radiotherapy, photothermal therapy (PTT), photodynamic therapy, sonodynamic therapy, and starvation therapy to treat tumors.[51–54] This combination therapy shows a synergistic anti-tumor effect of "1+1>2", rather than a simple additive effect. The combination of CDT and PTT has also been extensively studied. PTT is a physiotherapeutic method that artificially raises tissue temperature to exploit the sensitivity of cells to heat to induce apoptosis or increase their sensitivity to radiation or chemotherapy. PTT exhibits great promise because it can absorb light energy in a photothermal agent and then convert it to heat energy at the tumor site so that the temperature of the tumor site can be raised to cause hyperthermia to kill tumor cells.[55–58] Although PTT has the advantages of high efficiency, non-invasive, and no systematic side effects, it is difficult to eliminate tumor cells by using PTT alone. The efficiency of Fenton/Fenton-like reaction can be enhanced through photothermal effects. Thus, combining PTT and CDT with increased temperature will accelerate the generation of ·OH, thereby improving the therapeutic effect. Therefore, it is meaningful to explore a therapeutic approach that combines PTT and CDT.[59]

At present, the treatment means for cancer in the clinic is still relatively single, and there are disadvantages such as large trauma, tumor drug resistance, and incomplete resection of tumors leading to recurrence. Noble metal nanomaterials have been investigated in the biomedical field due to their good biocompatibility, local surface plasmon resonance effect, and strong light absorption and catalytic capabilities.[60,61] Noble metal nanomaterials can be targeted and aggregated in the tumor region, significantly improving treatment efficiency. Exploring the combined use of noble metal nanomaterials in CDT and PTT combination therapies to maximize the efficiency of the Fenton reaction and the level of ROS generation, as well as to improve ROS-mediated therapies, has instructive implications for cancer treatment. The obvious absorption of precious metal nanomaterials in the near-infrared light region is expected to be applied not only in PTT but also in CDT combined with PTT. The platinum-based alloys with excellent photothermal conversion and enzyme-like activity can be used to increase temperature, GSH depletion and O_2 production in the TEM.[49] Herein, bimetallic PtMn nanocubes were rationally designed and utilized to explore the efficiency of CDT/PTT synergistic treatment. PtMn nanocubes were easily synthesized by a one-step high-temperature pyrolysis process, by controlling both the nucleation process and the subsequent crystal growth stage. Then, polyethylene glycol (PEG) was modified to the monodisperse PtMn nanocubes to enhance biocompatibility. Benefiting from the alloying of Pt with Mn doping, the structure of the electron cloud has changed, resulting in different degrees of the shift in electron binding energy, which is a major factor in increasing the Fenton reaction activity. The PtMn nanocubes catalyzed endogenous H_2O_2 to toxic ·OH in mild acid TME. Meanwhile, the intrinsic GSH depletion activity of PtMn nanocubes consumed GSH with the assistance of Mn^{3+} and Mn^{2+}, which were the exact results of the Fenton reaction. The mild temperature due to the surface plasmon resonance (SPR) effect of Pt metal can also enhance the Fenton reaction. Thus, PtMn nanocubes can not only destroy the

antioxidant system via efficient ROS generation and continuous GSH consumption but also propose the photothermal effect of noble metal for enhanced Fenton reaction activity.

Materials and Methods

Materials

Manganese carbonyl ($Mn_2(CO)_{10}$), platinum acetylacetonate ($Pt(acac)_2$), octadecene, oleylamine (OAm), oleic acid (OA), hexane, isopropanol, 3.3′,5,5′-tetramethyl-benzidine (TMB), 5.5'-Dithiobis (2-nitrobenzoic acid) (DTNB), 5.5-dimethyl-1-pyrrolin-n-oxide (DMPO), propidium iodide (PI, 98%) were obtained from Aladdin (Shanghai, China). Rhodamine B (RhB), 2.7-dichlorofluorescein diacetate (DCFH-DA), and calcein-acetoxymethyl ester (AM, 97%) were obtained from Beyotime Biotechnology Co. Ltd. Thiol TrackerTM Violet and Dulbecco's modified Eagle medium (DMEM) were obtained from Thermo Fisher Scientific.

Synthesis and Characterization of the Bimetallic PtMn Nanocubes

At first, 0.1 g of $Pt(acac)_2$, 10 mL of octadecene, 1 mL of OA, and 1 mL of OAm were mixed under magnetic stirring and N_2 atmosphere. The mixture was then heated to 70 °C for totally dissolved $Pt(acac)_2$, and then, the temperature was maintained at around 180 °C. Next, the solution of $Mn_2(CO)_{10}$ in hexane was rapidly injected into the above solution, and the solution was maintained at 200 °C for 1 hour. In the end, polyethylene glycol (amine)-2000 ($PEG\text{-}NH_2$) was modified on the synthesized material.

X-ray diffraction (XRD) patterns were obtained using a RigakuD/max-TTR-III diffractometer. Morphology and element mapping of as-synthesized materials were obtained using a PHILIPS-CM-20-FEG transmission electron microscope (TEM). The chemical composition of the synthesized materials was analyzed using an ESCALAB XI+ X-ray photoelectron spectrometer (XPS).

Fenton Reaction Properties

For detection of ROS generation by PtMn nanocubes with or without NIR irradiation, the specific amount of PtMn nanocubes, TMB, and H_2O_2 were dispersed in 3.0 mL of PBS (pH=5.8, 7.0, and 7.8). The UV-vis characteristic absorption peak was detected at 650 nm. The ROS generated by Pt and PtMn nanocubes in different processes were also evaluated using an ESR spectrometer. DMPO was utilized as a trapping agent to investigate the activity of ·OH.

GSH Depletion Properties

500 μg mL^{-1} of PtMn nanocubes and 500 μg mL^{-1} Pt nanocubes were added into GSH aqueous solution. Then 0.2 mM of DTNB was added to detect the -SH group.

Photothermal Performance

The PtMn nanocubes with different concentrations were prepared and then irradiated under a NIR (808 nm) laser for 300 s. The temperature changes and infrared thermal images were recorded.

In vitro Anti-Tumor Efficiency

Human hepatocellular carcinoma cells (Huh7 cells) and mouse epithelial fibroblasts (L929 cells) purchased from the Cell Bank of the Chinese Academy of Sciences (Shanghai, China) were cultured in DEME. All cell lines were maintained in an incubator at 37 °C and 5% CO_2. At first, the cellular uptake performance of PtMn nanocubes was investigated using RhB-labeled PtMn nanocubes. Then, the biocompatibility and cytotoxicity analysis was performed using the MTT reagent. The cells were seeded at a density of 5000 cells per well in 96-well plates, and then, incubated with different concentrations of PtMn. Subsequently, 20 μL of MTT solution (5 mg mL^{-1}) was added to each well and incubated with the cells for 4 hours. Afterward, 100 μL of DMSO was added to each well and incubated for another 20 min. The absorbance at 490 nm was measured to calculate the cell survival rate.

For evaluation of the ROS generation, GSH depletion, and O_2 generation abilities of PtMn nanocubes, Huh7 cells were seeded into 6-well a plate overnight and distributed into four groups: (1) control, (2) NIR, (3) PtMn, and (4) PtMn +NIR. The PtMn were allowed to incubate with cells for 4 h, followed by the cells being treated with NIR (0.8 W cm^{-2}) for 5 min. The DCFH-DA was added to individual culture dishes for 15 min and washed with PBS. Subsequently, Hoechst 33,342 as a nucleus fluorescence probe was incubated with Huh7 cells for 10 min and washed with PBS. Finally, a laser scanning confocal microscope (CLSM) was used for observing the cells. The intracellular GSH depletion and O_2 generation were characterized by the commercial Thiol Tracker Violet probe and corresponding trapping agent $[Ru(dpp)_3]Cl_2$, respectively. The cytotoxicity of PtMn nanocubes was investigated using AM/PI assays.

In vivo Anti-Tumor Efficiency

The animal study protocol was approved by the Ethics Committee of Guangxi Medical University Cancer Hospital (protocol code KY 2022–129/130 and approved on 25 February 2022) for studies involving animals. Animal ethics review follows the Guiding Opinions on the Treatment of Laboratory Animals issued by the Ministry of Science and Technology of the People's Republic of China and the Laboratory Animal-Guideline for Ethical Review of Animal Welfare issued by the National Standard GB/T35892-2018 of the People's Republic of China. Firstly, the Huh7 tumor-bearing Blab/c nude mice were then intravenously injected with PtMn nanocubes (20 mg kg^{-1}), and the mice were sacrificed at 3, 6, 12, 24, and 48 h post-injection. The biodistribution of PtMn nanocubes in different organs and tumors was calculated as the Mn percentage. Then, the tumor model was established by subcutaneous inoculating of Huh7 cells (100 μL, 5.0×10^6 cells) at the right posterior of the mice. The mice were randomly divided into four groups (n = 5): (1) control, (2) NIR, (3) PtMn, and (4) PtMn+NIR. The intravenously injected dose was 100 μL (20 mg kg^{-1}). Afterward, the body weights and tumor sizes of the mice were recorded. After 14 days, the collected tumors were stained with H&E staining, and observed by using the laser scanning microscopy (CLSM).

Results and Discussion

PtMn nanocubes were synthesized via a one-step high-temperature pyrolysis process, involving both the nucleation process control and the subsequent crystal growth stage. The PEG was modified to enhance biocompatibility. The zeta potentials of PtMn without PEG modification and PtMn with PEG modification are shown in Figure S1. The zeta potential of PtMn without PEG modification was −1.49 ± 0.62 mV, and that of PtMn with PEG modification was −4.83 ± 0.57 mV. Both zeta potentials are negative, but PtMn with PEG modification has a smaller value indicating better dispersibility. PtMn was dissolved in PBS solution (pH = 5.8) for 8 days, and then the polydispersity index (PDI) values were recorded for different periods (Figure S2). With increasing time, the PDI of PtMn in PBS solution gradually decreased, and the molecular weight distribution gradually became uniform, indicating that the PtMn nanocubes were stable The average particle size of PtMn nanocubes was about 18.23 nm as indicated by the TEM image (Figure 1a). The particle size decreased gradually with the increase of Mn doping ratios. The decrease in the particle size of nanoparticles may be caused by the inhibition effect of PtMn nanocubes growth by Mn cation (Figure 1b). In the synthesis experiments, we optimized the molar ratio of Pt:Mn. When the molar ratio of Pt:Mn is 1:3, the PtMn nanocubes were optimal uniform for further application. Selected area electron diffraction (SAED) of PtMn nanocubes was displayed in Figure 1c. Furthermore, elemental mapping based on high-angle annular dark-field scanning TEM revealed the uniform distribution of Pt and Mn elements (Figure 1d and e). The XRD pattern of the PtMn nanocubes showed that the characteristic diffraction peaks, roughly coinciding with the standard cubic phase Pt (JCPDS No. 04–0802) with (111), (200), and (220) lattice planes assigned to the characteristic diffraction peaks at 40.12°, 46.67°, and 68.12°, respectively (Figure 1f). The diffraction patterns indicate that the particles have a Face-Centered Cubic structure. To further understand the chemical composition of the PtMn nanocubes, XPS analysis was performed. The XPS elemental valence analysis in Figure S3 shows the presence of Pt elements in the form of Pt 4f, as well as Mn $2p_{3/2}$ and Mn $2p_{1/2}$ peaks located at 641.4 and 654.4 eV.

Considering the Fenton reaction performance of PtMn nanocubes, the generation of ·OH was investigated by TMB in the condition of H_2O_2. Mn doping can enhance the degradation of H_2O_2 by PtMn nanocubes, which further enhances the Fenton reaction efficacy. Acidic conditions are more favorable for PtMn nanocubes to catalyze the generation of ·OH

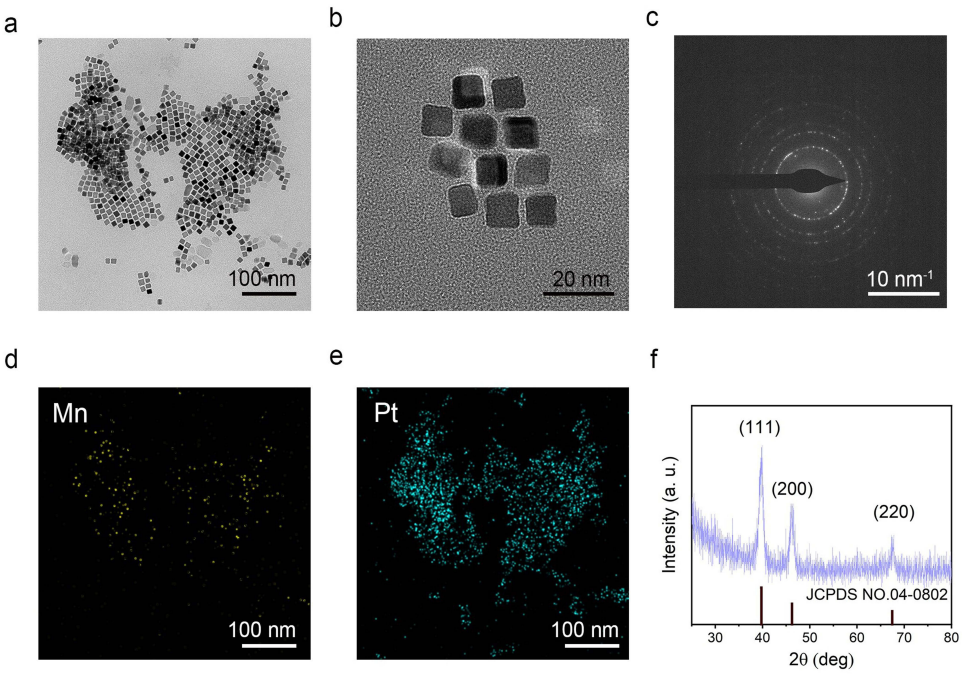

Figure 1 (**a** and **b**) TEM images of PtMn nanocubes. (**c**) SAED pattern of PtMn nanocubes. (**d** and **e**) Mn and Pt element mappings of PtMn nanocubes. (**f**) XRD pattern of PtMn nanocubes.

from endogenous H_2O_2 (Figure 2a). Compared with the control group, PtMn+NIR showed a significant chemodynamic effect (Figure 2b). Especially, upon 808 nm laser irradiation, the characteristic peak at 650 nm of oxTMB was improved, indicating that the NIR can promote the production of ·OH. In the Fenton reaction, the energy of NIR promoted the efficiency of electron transfer and accelerated the effect of the Fenton reaction. The PtMn nanocubes also exhibited a time-dependent chemodynamic effect (Figure 2c and d). The catalytic kinetic parameters of PtMn nanocubes were conducted with the Michaelis-Menten model (Figure 2e and f), where the K_m and V_{max} were 1.78×10^{-8} M s^{-1} and 84.19 mM, respectively. The generation of ·OH was also confirmed by electron spin resonance (ESR). DMPO was used to detect ·OH. From the ESR spectra, the characteristic signal peaks featured with the intensity of 1:2:2:1 belonged to ·OH, which confirmed the generation of ·OH (Figure 2g). Compared to Pt nanocubes, PtMn has a higher capacity to generate ·OH. The GSH depletion ability of PtMn nanocubes was investigated by employing DTNB as an indicator (Figure 2h and i). The absorbance at 412 nm decreased with increasing incubation time. At the same incubation time of 40 min, PtMn showed lower GSH content than Pt nanocubes. The capacity of GSH depletion properties for ROS amplification was confirmed. Thus, as the catalytic activity of single noble metal materials is limited by their intrinsic electronic structure and limited electron transfer, the cost of alloyed noble metal nanoparticles can be reduced by the addition of non-precious metals, which will enhance the Peroxidase-like enzyme activity of the alloys due to their synergistic effect.

As an alloy material, PtMn nanocubes may have high photothermal performance. The photothermal conversion performance and photothermal stability of PtMn nanocubes were characterized in detail. The temperature of the different concentrations (0, 25, 50, 100, and 200 μg mL^{-1}) of PtMn nanocubes solution was recorded after 808 nm laser irradiation for 10 min (Figure 3a and c). As the concentration of PtMn nanocubes increased, the heating rate increased, indicating that the photothermal effect of PtMn nanocubes was concentration-dependent. Then, the temperature increase of PtMn nanocubes solution at different laser powers (0.5, 1.0, 1.5, and 2.0 W cm^{-2}) was also recorded. We selected 1.5 W cm^{-2} as the appropriate laser power for mild photothermal in vitro, which showed less damage to normal tissues. Under the irradiation of different laser powers, the temperature of the PtMn nanocubes increased from room temperature to 33.4°C, 40.7°C, 48.9 °C, and 56.5°C, respectively (Figure 3b). The rising and cooling temperature curve of PtMn nanocubes was measured at a concentration of 200 μg mL^{-1} under 1.5 W cm^{-2} through the cooling stage (Figure 3d), it was calculated

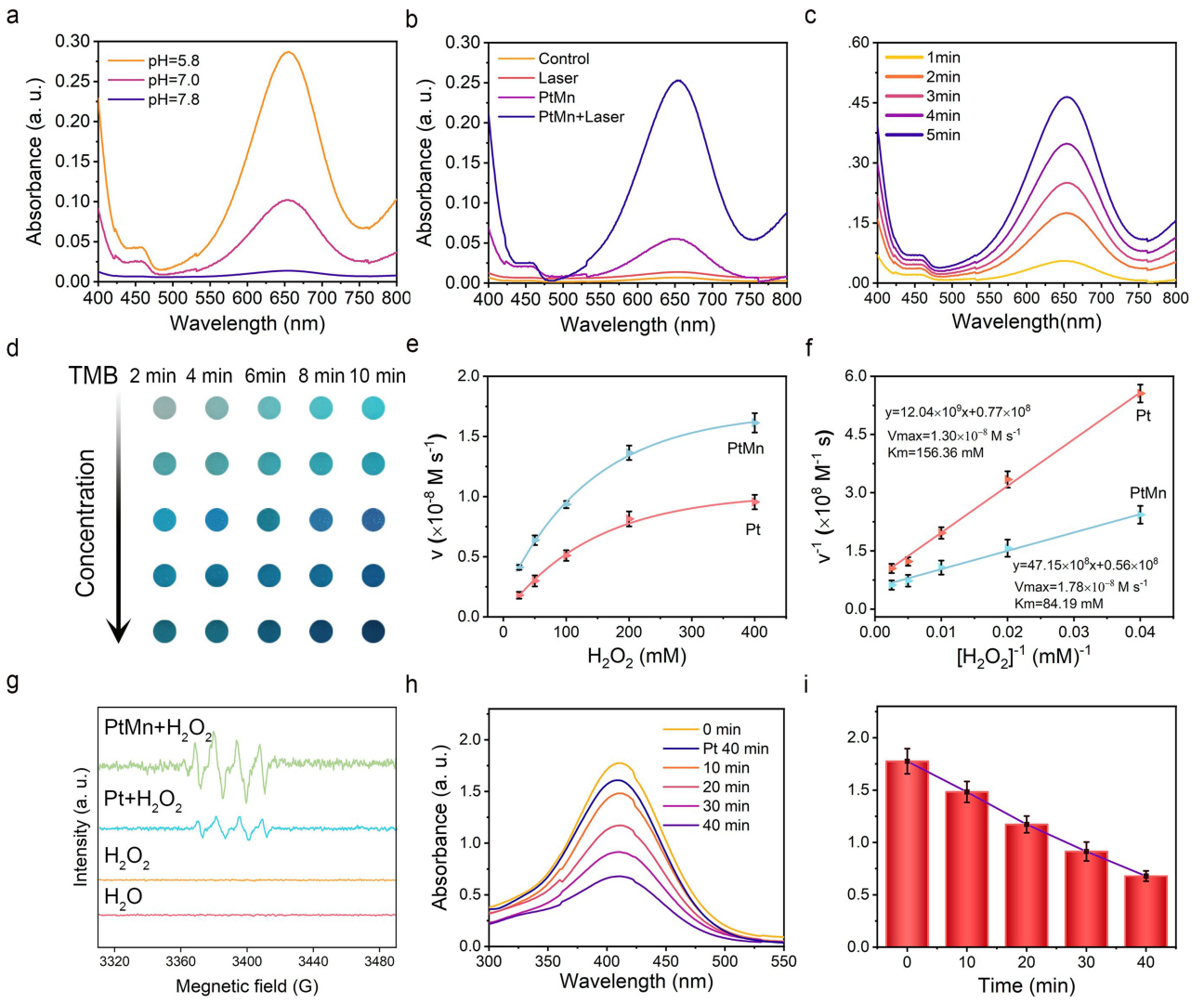

Figure 2 (**a**) UV-vis absorption spectra of oxTMB catalyzed by PtMn nanocubes under different pH conditions. (**b**) UV-vis absorption spectra of oxTMB catalyzed by PtMn nanocubes in different groups. (**c**) UV-vis absorption spectra of oxTMB catalyzed by PtMn nanocubes with time increase. (**d**) The color photo of oxTMB catalyzed by PtMn nanocubes. (**e**) Michaelis-Menten curves and (**f**) Lineweaver-Burk plots of Pt and PtMn nanocubes. Data presented as mean ± standard deviation (n = 3). (**g**) ESR spectra of ·OH in PtMn+H_2O_2 and Pt+H_2O_2 nanocubes. (**h**) UV-vis absorption spectra of DTNB catalyzed by Pt and PtMn nanocubes. (**i**) Quantitative analysis of (**h**).

that the T_s was 183 s and the photothermal conversion efficiency was 32.6%. After four cycles of increasing and rolling, the photothermal stability of PtMn nanocubes was maintained well (Figure 3e).

Then, encouraged by the excellent Fenton reaction properties and NIR-irradiated photothermal effect of PtMn nanocubes, the anticancer therapeutic effect of PtMn nanocubes at the cellular level was investigated in detail. At first, the endocytosis of PtMn nanocubes was first investigated before evaluating the biocompatibility. The Huh7 cells were incubated with PtMn nanocubes modified by RhB. Figure 4a showed that PtMn nanocubes were gradually engulfed by the Huh7 cells in a time-dependent manner. The red fluorescence of RhB-PtMn nanocubes began to coincide after 2 h of incubation. At 4 h after incubation, the red fluorescence of RhB-PtMn nanocubes was the highest, demonstrating the efficiency of the cellular uptake performance. Then, the biocompatibility and toxicity of PtMn nanocubes were initially assessed at the cellular level. Normal L929 cells and Huh7 tumor cells were selected as two representative cell lines. As shown in Figure 4b, the L929 cells presented no significant cell death even the concentration of PtMn nanocubes up to 200 μg mL^{-1}. As shown in Figure 4c, the Huh7 cells in the PtMn+NIR group (200 μg mL^{-1}) presented the lowest cell viability around 25%.

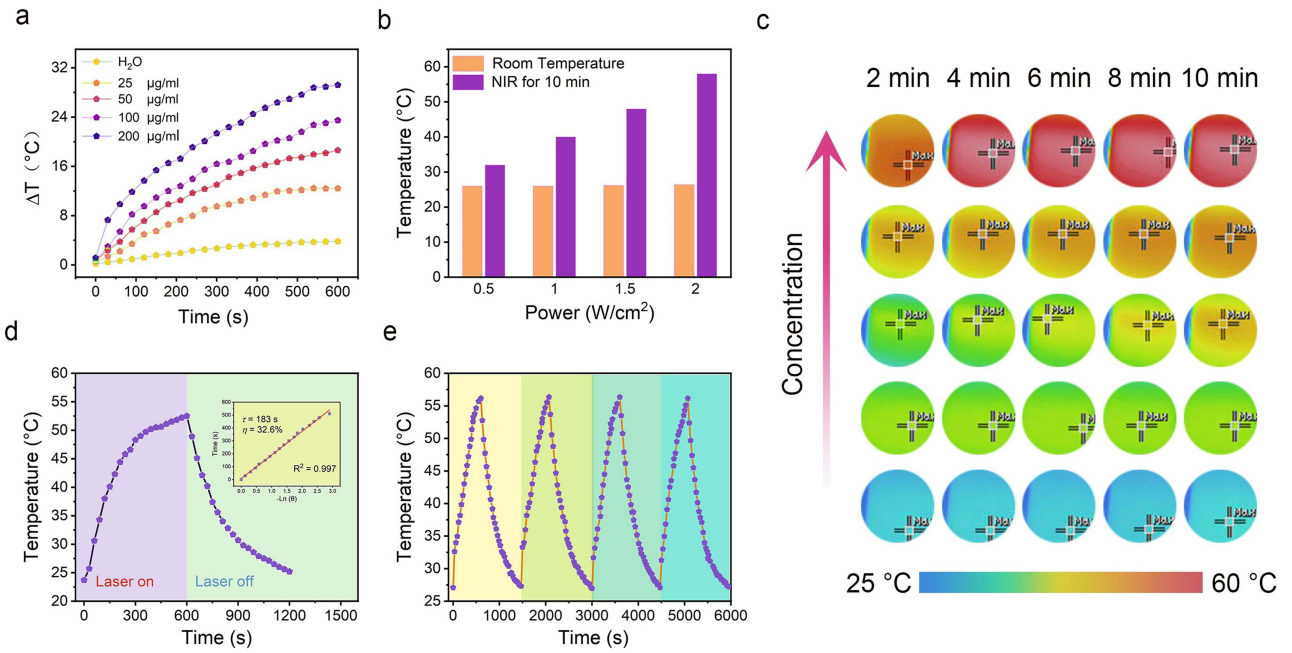

Figure 3 (**a**) The photothermal effect of PtMn nanocubes with different concentrations. (**b**) The temperature increase of PtMn nanocubes under different laser powers. (**c**) Infrared thermal imaging of PtMn nanocubes under different concentrations with time increase. (**d**) The photothermal conversion efficiency of PtMn nanocubes. (**e**) The photothermal stability of PtMn nanocubes.

Next, the production of intracellular ROS was evaluated by using a chemical probe DCFH-DA, which emits green fluorescence attributed to oxidized DCF. In Figure 4d, the PtMn+NIR group had the strongest green fluorescence signal, suggesting that the PtMn+NIR group showed a higher level of intracellular ROS than other groups. The GSH content results showed that the PtMn group had higher GSH consumption than the PtMn+NIR group. The production of O_2 catalyzed by PtMn nanocubes in Huh7 cells was also investigated using $[Ru(dpp)_3]Cl_2$ as an O_2 indicator. In Figure 4d, the group of PtMn and PtMn+NIR exhibit a weak red fluorescence signal compared with the control group, suggesting that the photothermal effect could relieve hypoxia. For distinguishing live cells from dead cells visually, co-staining with calcein-AM/PI was performed. As shown in Figure 4d, in the control a majority of the dead cells were observed in the PtMn group and the PtMn+NIR group, and the PtMn+NIR group showed the highest proportion of dead cells due to the ROS generation performance and GSH consumption performance.

Subsequently, to investigate the in vivo antitumor therapeutic performance of PtMn nanocubes, the Balb/c nude mice were selected for subcutaneous injection of Huh7 cells on the right side to establish a Huh7 tumor model. At first, the biological distribution of PtMn nanocubes was performed. After the intravenous injection of PtMn nanocubes (20 mg kg^{-1} of mouse body weight), major organs and tumor tissues were collected at different time points (3, 6, 12, 24, and 48 h). The Mn content in different tissues was determined by ICP-OES. It can be seen that PtMn nanocubes accumulated in the liver, spleen, kidney, and tumor sites effectively after tail vein injection (Figure 5a), demonstrating that PtMn nanocubes could be captured by the reticuloendothelial system, which reached the maximum at 6 h post-injection and then began to decline. The enhanced penetration and retention effect causes the accumulation of PtMn nanocubes at the tumor site. Then, the antitumor effect of PtMn nanocubes was investigated by using the Huh7 tumor-bearing mice. Huh7 tumor-bearing mice were randomly divided into four experimental groups: 1) control, 2) NIR, 3) PtMn, and 4) PtMn +NIR. When the tumor volume was grown to about 100 mm^3, normal saline, PtMn nanocubes were injected through the tail vein on days 1, 4, and 7, respectively. After 12 h, the external NIR laser was applied. The PtMn+NIR group presented the obvious tumor inhibition effect based on the relative tumor volume growth curves (Figures 5b and c), confirming that PtMn nanocubes irradiated with NIR had an excellent tumor treatment effect. After 10 minutes of irradiation, the temperature of the tumor site rapidly increased to more than 45 °C, confirming the photothermal performance of PtMn (Figure S4). Especially, as shown in Figure 5d, mice in all groups showed a consistent trend of weight gain throughout

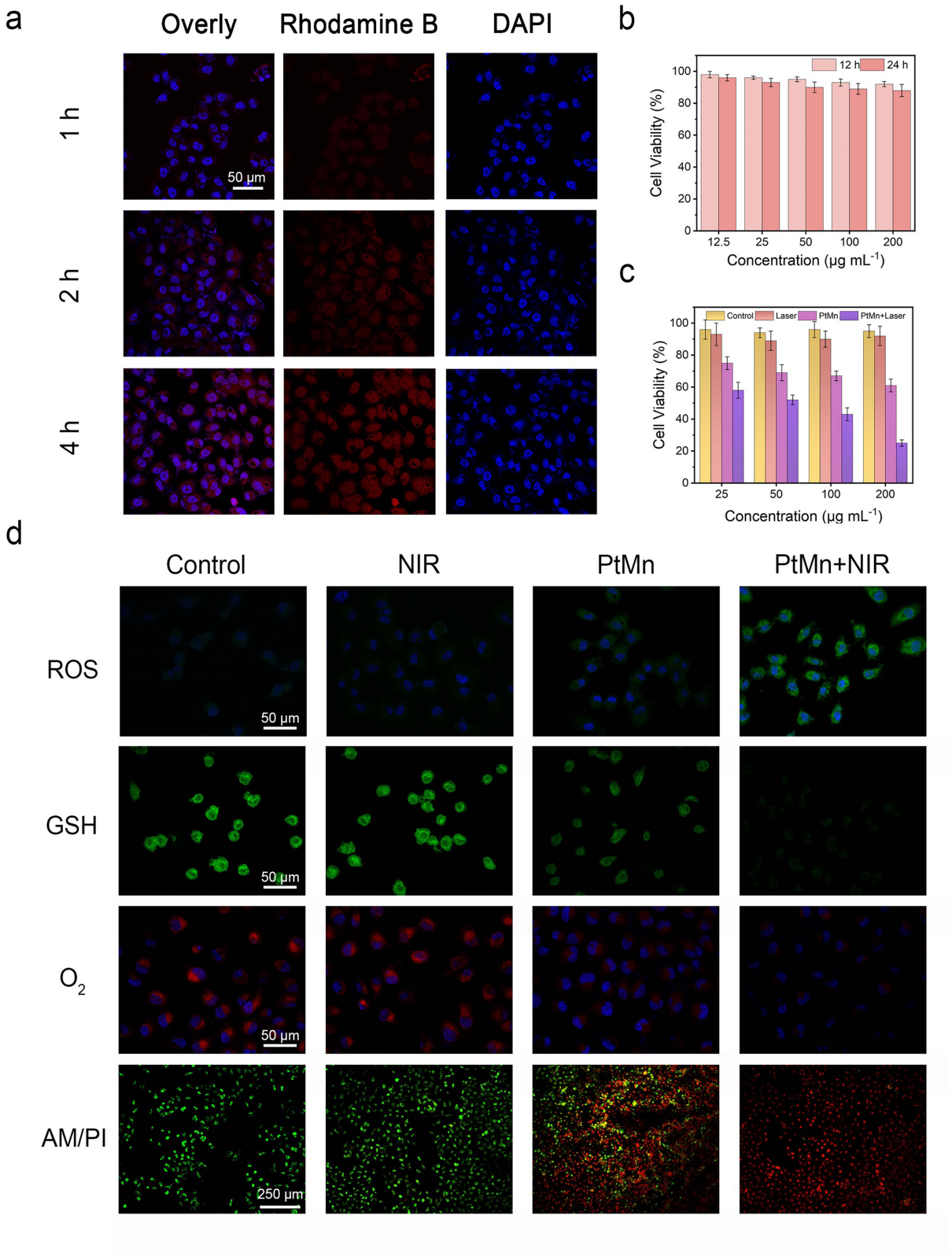

Figure 4 (**a**) Cellular uptake performance of RhB-label PtMn nanocubes. (**b** and **c**) MTT assay of PtMn nanocubes on L929 and Huh7 cells, respectively, for biocompatibility and cytotoxicity estimation. (**d**) ROS generation, GSH depletion, O_2 generation abilities of PtMn nanocubes, and live/dead cell staining.

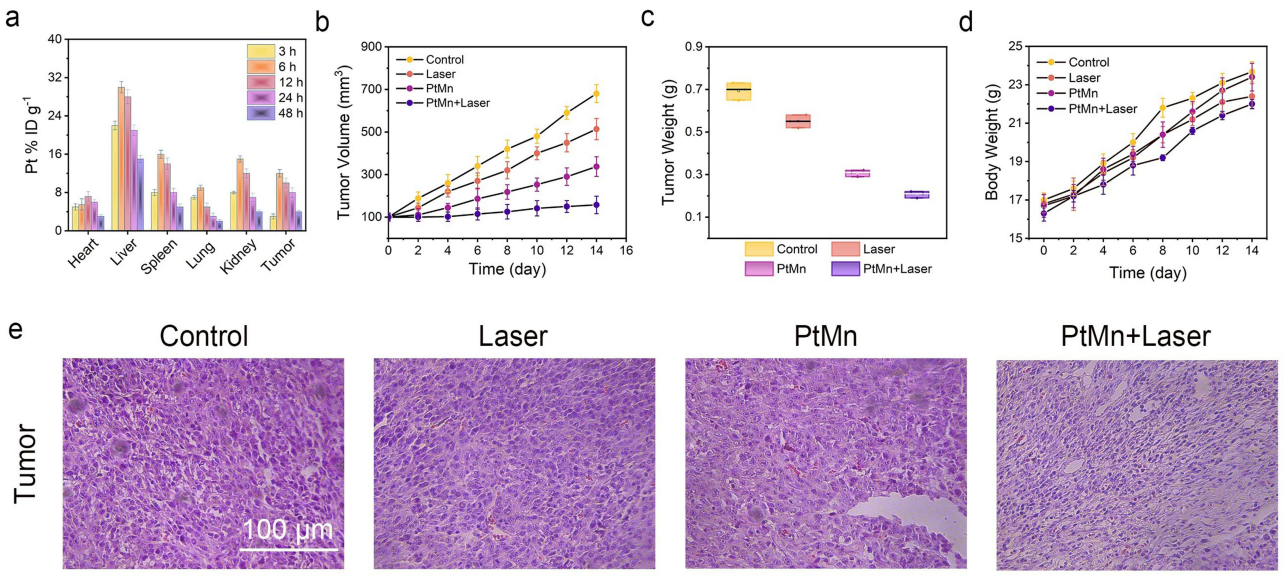

Figure 5 (**a**) Biodistribution of Pt in main organs and tumors. (**b**) Tumor volume and (**c**) tumor weight in different groups. Data presented as mean ± S.D. (n = 5). (**d**) The body weight of mice in different groups. Data presented as mean ± S.D. (n = 5). (**e**) H&E-staining assay of tumor tissues.

the whole treatment process. In Figure S5, the tumor growth in the PtMn+NIR group were significantly inhibited compared to the other groups. It can be seen that the combined CDT/PTT effect in the PtMn+NIR group resulted in the strongest inhibition of tumor growth. The efficacy of the CDT/PTT synergistic therapy was also demonstrated by H&E staining, which was consistent with tumor volume curves (Figure 5e). The tissue section in the PtMn+NIR group showed the lowest nuclear staining rate, the tumor cells were destroyed in the PtMn+NIR treatment group, indicating that it has a positive tumor treatment effect. The mice in the PtMn+NIR group still maintained a 60% survival rate even after 40 days of treatment, while the mice in the other treatment all died within 15–32 days, suggesting the good therapeutic effect and biosafety of PtMn+NIR group (Figure S6).

Conclusion

The study reports the successful preparation of bimetallic PtMn nanocubes for a CDT/PTT synergistic therapeutic strategy. In the photothermal properties of the PtMn nanocubes, the photothermal conversion efficiency can be as high as 32.6% and the photothermal stability of the PtMn nanocube was well maintained. PtMn nanocubes exhibit the characteristics of ROS bloom and GSH depletion. The PtMn nanocubes can catalyze endogenous H_2O_2 to toxic ·OH in a mild acid TME. Simultaneously, Mn^{3+}/Mn^{2+} can help consume the inner antioxidant GSH in the tumor. The SPR effect of Pt metal can provide mild temperature to enhance the Fenton reaction of PtMn nanocubes. Therefore, the PtMn nanocubes prepared in this study can enhance the Fenton reaction activity by utilizing the photothermal effect to achieve effective combined CDT/PTT for tumor treatment. In conclusion, PtMn nanocubes were prepared for CDT/PTT combination therapy in cancer treatment. This provides a solid foundation for the use of noble metal nanomaterials in cancer therapy.

Acknowledgments

The author(s) declare financial support was received for the research, authorship, and/or publication of this article. This research was funded by the National Natural Science Foundation (Grant No. 82260580), the Key R&D Program of Scientific Research and Technology Development Project of Guangxi (Grant No. 2022AB11046), the Key R&D Program of Scientific Research and Technology Development Project of Nanning, Guangxi (Grant No. ZC20213009), the Key R&D Program of Scientific Research and Technical Development Project of Qingxiu District, Nanning, Guangxi (Grant

No. 2021015), the Youth Science Foundation of Guangxi Medical University (No. GXMUYSF 202318) and Guangxi Medical and health key discipline construction project.

Author Contributions

All authors made a significant contribution to the work reported, whether that is in the conception, study design, execution, acquisition of data, analysis and interpretation, or in all these areas; took part in drafting, revising or critically reviewing the article; gave final approval of the version to be published; have agreed on the journal to which the article has been submitted; and agree to be accountable for all aspects of the work.

Disclosure

The authors report no conflicts of interest in this work.

References

1. Yang B, Chen Y, Shi J. Reactive Oxygen Species (ROS)-Based Nanomedicine. *Chem Rev*. 2019;119(8):4881–4985. doi:10.1021/acs.chemrev.8b00626
2. Sang W, Zhang Z, Dai Y, Chen X. Recent advances in nanomaterial-based synergistic combination cancer immunotherapy. *Chem. Soc. Rev.* 2019;48(14):3771–3810. doi:10.1039/C8CS00896E
3. Huang Y, Ren J, Qu X. Nanozymes: classification, Catalytic Mechanisms, Activity Regulation, and Applications. *Chem. Rev.* 2019;119(6):4357–4412. doi:10.1021/acs.chemrev.8b00672
4. Li Z, Zou J, Chen X. In Response to Precision Medicine: current Subcellular Targeting Strategies for Cancer Therapy. *Adv. Mater.* 2023;35(21):2209529.
5. Gil JF, Moura CS, Silverio V, Goncalves G, Santos HA. Cancer Models on Chip: paving the Way to Large-Scale Trial Applications. *Adv. Mater.* 2023;35(35). doi:10.1002/adma.202300692
6. Kohls A, Maurer Ditty M, Dehghandehnavi F, Zheng SY. Vertically Aligned Carbon Nanotubes as a Unique Material for Biomedical Applications. *ACS Appl Mater Interfaces*. 2022;14(5):6287–6306. doi:10.1021/acsami.1c20423
7. Zhang J, Huang L, Ge G, Hu K. Emerging Epigenetic-Based Nanotechnology for Cancer Therapy: modulating the Tumor Microenvironment. *Adv Sci (Weinh)*. 2023;10(7):e2206169. doi:10.1002/advs.202206169
8. Liu H, Zhao J, Xue Y, et al. X-Ray-Induced Drug Release for Cancer Therapy. *Angew Chem Int Ed Engl*. 2023;62(39):e202306100. doi:10.1002/anie.202306100
9. Kaltbeitzel J, Wich PR. Protein-based Nanoparticles: from Drug Delivery to Imaging, Nanocatalysis and Protein Therapy. *Angew. Chem. Int. Ed.* 2023;62(44). doi:10.1002/anie.202216097
10. Jiang S, Chen X, Lin J, Huang P. Lactate-Oxidase-Instructed Cancer Diagnosis and Therapy. *Adv. Mater.* 2023.
11. Zhuang F, Xiang H, Huang B, Chen Y. Ultrasound-Triggered Cascade Amplification of Nanotherapy. *Adv. Mater.* 2023;35(33). doi:10.1002/adma.202303158
12. Zhen W, Weichselbaum RR, Lin W. Nanoparticle-Mediated Radiotherapy Remodels the Tumor Microenvironment to Enhance Antitumor Efficacy. *Adv Mater*. 2023;35(21):e2206370. doi:10.1002/adma.202206370
13. Zhao P, Li H, Bu W. A Forward Vision for Chemodynamic Therapy: issues and Opportunities. *Angew. Chem. Int. Ed.* 2023;62(7):e202210415.
14. Zhang MJ, Wang YY, Han LL, et al. Biomaterials Elicit Pyroptosis Enhancing Cancer Immunotherapy. *Adv. Funct. Mater.* 2023.
15. Zhang K, Qi C, Cai K. Manganese-Based Tumor Immunotherapy. *Adv Mater*. 2023;35(19):e2205409. doi:10.1002/adma.202205409
16. Zhang H, Mao Z, Kang Y, Zhang W, Mei L, Ji X. Redox regulation and its emerging roles in cancer treatment. *Coord. Chem. Rev.* 2023;475.
17. Yang H, Yao X, Liu Y, Shen X, Li M. Ferroptosis Nanomedicine: clinical Challenges and Opportunities for Modulating Tumor Metabolic and Immunological Landscape. *Acs Nano*. 2023;17(16):15328–15353. doi:10.1021/acsnano.3c04632
18. Yang F, Dong J, Li Z, Wang Z. Metal-Organic Frameworks (MOF)-Assisted Sonodynamic Therapy in Anticancer Applications. *ACS Nano*. 2023;17(5):4102–4133. doi:10.1021/acsnano.2c10251
19. Wibrianto A, Getachew G, Direrssa WB, et al. A multifunctional nanocatalyst based on ultra-fluorescent carbon quantum dots for cascade enzymatic activity and stimuli-responsive chemotherapy of cancer. *Carbon*. 2023;208:191–207. doi:10.1016/j.carbon.2023.03.052
20. Yang D, Tang Y, Zhu B, et al. Engineering Cell Membrane-Cloaked Catalysts as Multifaceted Artificial Peroxisomes for Biomedical Applications. *Adv Sci (Weinh)*. 2023;10(17):e2206181. doi:10.1002/advs.202206181
21. Wang Z, Jin A, Yang Z, Huang W. Advanced Nitric Oxide Generating Nanomedicine for Therapeutic Applications. *ACS Nano*. 2023;17(10):8935–8965. doi:10.1021/acsnano.3c02303
22. Song X, Zhang Q, Chang M, et al. Nanomedicine-Enabled Sonomechanical, Sonopiezoelectric, Sonodynamic, and Sonothermal Therapy. *Adv. Mater.* 2023;35(31). doi:10.1002/adma.202212259
23. Overchuk M, Weersink RA, Wilson BC, Zheng G. Photodynamic and Photothermal Therapies: synergy Opportunities for Nanomedicine. *ACS Nano*. 2023;17(9):7979–8003. doi:10.1021/acsnano.3c00891
24. Ma J, Zhang L, Lei B. Multifunctional MXene-Based Bioactive Materials for Integrated Regeneration Therapy. *ACS nano*. 2023;17(20):19526–19549. doi:10.1021/acsnano.3c01913
25. Chang M, Hou Z, Wang M, Li C, Al Kheraif AA, Lin J. Tumor Microenvironment Responsive Single-Atom Nanozymes for Enhanced Antitumor Therapy. *Chemistry*. 2022;28(15):e202104081. doi:10.1002/chem.202104081
26. Zhou Y, Fan S, Feng L, Huang X, Chen X. Manipulating Intratumoral Fenton Chemistry for Enhanced Chemodynamic and Chemodynamic-Synergized Multimodal Therapy. *Adv Mater*. 2021;33(48):e2104223. doi:10.1002/adma.202104223

27. Zhixin Z, Margarita V-G, Itamar W. Stimuli-responsive metal–organic framework nanoparticles for controlled drug delivery and medical applications. *Chem. Soc. Rev.* 2021.
28. Zhang Y, Zhang X, Yang H, et al. Advanced biotechnology-assisted precise sonodynamic therapy. *Chem. Soc. Rev.* 2021.
29. Yu F, Shange L, Yu Y, Hongpan R, Jiatao Z. Catalytic Nanomaterials toward Atomic Levels for Biomedical Applications: from Metal Clusters to Single-Atom Catalysts. *ACS Nano*. 2021.
30. Yang Y, Wu H, Liu B, Liu Z. Tumor microenvironment-responsive dynamic inorganic nanoassemblies for cancer imaging and treatment. *Adv Drug Deliv Rev*. 2021;179:114004. doi:10.1016/j.addr.2021.114004
31. Xujiang Y, Xinyi L, Kai Y, et al. (Sb, Bi)-Based Nanomaterials for Cancer Imaging and Therapy: a Materials Perspective. *ACS Nano*. 2021.
32. Xu C, Pu KY. Second near-infrared photothermal materials for combinational nanotheranostics. *Chem. Soc. Rev.* 2021;50(2):1111–1137. doi:10.1039/D0CS00664E
33. Zhu Y, Gong P, Wang J, et al. Amplification of Lipid Peroxidation by Regulating Cell Membrane Unsaturation To Enhance Chemodynamic Therapy. *Angew. Chem. Int. Ed.* 2023;62(12):e202218407.
34. Zhu P, Zhou C, Chen J, et al. Propionibacterium acnes Cloaked with ZnAl Layered Double Hydroxides Synergistically Inhibits Tumor Growth and Metastasis. *Adv. Funct. Mater.* 2023;33(25):2214105.
35. Zhang H, Chen Y, Hua W, et al. Heterostructures with Built-in Electric Fields for Long-lasting Chemodynamic Therapy. *Angew Chem Int Ed Engl*. 2023;62(15):e202300356. doi:10.1002/anie.202300356
36. Zhao P, Jiang Y, Tang Z, et al. Constructing Electron Levers in Perovskite Nanocrystals to Regulate the Local Electron Density for Intensive Chemodynamic Therapy. *Angew Chem Int Ed Engl*. 2021;60(16):8905–8912. doi:10.1002/anie.202100864
37. Tian F, Wang S, Shi K, et al. Dual-Depletion of Intratumoral Lactate and ATP with Radicals Generation for Cascade Metabolic-Chemodynamic Therapy. *Adv Sci (Weinh)*. 2021;8(24):e2102595. doi:10.1002/advs.202102595
38. Qian M, Cheng Z, Luo G, et al. Molybdenum Diphosphide Nanorods with Laser-Potentiated Peroxidase Catalytic/Mild-Photothermal Therapy of Oral Cancer. *Adv Sci (Weinh)*. 2021;e2101527.
39. Li X, Xiao H, Xiu W, et al. Mitochondria-Targeting MoS2-Based Nanoagents for Enhanced NIR-II Photothermal-Chemodynamic Synergistic Oncotherapy. *ACS Appl Mater Interfaces*. 2021;13(47):55928–55938. doi:10.1021/acsami.1c18311
40. Zhong X, Wang X, Cheng L, et al. GSH-Depleted PtCu3 Nanocages for Chemodynamic- Enhanced Sonodynamic Cancer Therapy. *Adv. Funct. Mater.* 2020;30(4):1907954. doi:10.1002/adfm.201907954
41. Zhang M, Liu X, Luo Q, et al. Tumor environment responsive degradable CuS@mSiO2@MnO2/DOX for MRI guided synergistic chemo-photothermal therapy and chemodynamic therapy. *Chem Eng J*. 2020;389.
42. Xu X, Zeng Z, Chen J, et al. Tumor-targeted supramolecular catalytic nanoreactor for synergistic chemo/chemodynamic therapy via oxidative stress amplification and cascaded Fenton reaction. *Chem Eng J*. 2020;390.
43. Zhu P, Pu Y, Wang M, Wu W, Qin H, Shi J. MnOOH-Catalyzed Autoxidation of Glutathione for Reactive Oxygen Species Production and Nanocatalytic Tumor Innate Immunotherapy. *J Am Chem Soc*. 2023;145(10):5803–5815. doi:10.1021/jacs.2c12942
44. Peng J, Du K, Sun J, et al. Photocatalytic Generation of Hydrogen Radical (H·) with GSH for Photodynamic Therapy. *Angew. Chem. Int. Ed.* 2023;62(9). doi:10.1002/anie.202214991
45. Liu J, Li M, Zhao Z, et al. GSH-responsive and O2-economizing virus-like nanocapsule for photothermal-augmented sonodynamic therapy. *Chem Eng J*. 2023;458.
46. Li Y, Lei N, Yao X, et al. Hijacking Endogenous Iron and GSH Via a Polyvalent Ferroptosis Agonist to Enhance Tumor Immunotherapy. *Adv. Funct. Mater.* 2023.
47. Direrса WB, Getachew G, Wibrianto A, et al. Molybdenum-oxo-sulfide quantum dot-based nanocarrier: efficient generation of reactive oxygen species via photo/chemodynamic therapy and stimulus-induced drug release. *J Colloid Interface Sci*. 2023;647:528–545. doi:10.1016/j.jcis.2023.05.099
48. Getachew G, Korupalli C, Rasal AS, Chang J-Y. ROS generation/scavenging modulation of carbon dots as phototherapeutic candidates and peroxidase mimetics to integrate with polydopamine nanoparticles/GOx towards cooperative cancer therapy. *Composites Part B*. 2021;226:109364. doi:10.1016/j.compositesb.2021.109364
49. Huo L, Zhu S, Zeng J, et al. Multivalence Manganese Mediated Dual ROS Generator for Augmented Chemodynamic Therapy and Activated Antitumor Immunogenic Responses. *ACS Mater Lett*. 2024;6(3):885–895. doi:10.1021/acsmaterialslett.3c01459
50. Yu H, Si P, Lu W, et al. Construction of Core–Shell MOF CSMnP with Enzyme-Like Activity for Chemotherapy and Chemodynamic Therapy. *Inorganic Chemistry*. 2023;62(44):18128–18135. doi:10.1021/acs.inorgchem.3c02579
51. Zhou H, Zhang Y, Zhang R, et al. A Tumor-Microenvironment-Activatable Molecular Pro-Theranostic Agent for Photodynamic and Immunotherapy of Cancer. *Adv Mater*. 2023;35(30):e2211485. doi:10.1002/adma.202211485
52. Zhao X, Cheng H, Wang Q, et al. Regulating Photosensitizer Metabolism with DNAzyme-Loaded Nanoparticles for Amplified Mitochondria-Targeting Photodynamic Immunotherapy. *ACS Nano*. 2023;17(14):13746–13759. doi:10.1021/acsnano.3c03308
53. Zhang W, Wang M, Liu B, et al. Rational design of Multi-model ROS regulation Nano-platform for enhanced Mild-temperature photothermal therapy. *Chem Eng J*. 2023;460.
54. Zhang W, Cai K, Sun Z, et al. Elevating Second Near-Infrared Photothermal Conversion Efficiency of Hollow Gold Nanorod for a Precise Theranostic of Orthotopic Bladder Cancer. *ACS nano*. 2023;17(19):18932–18941. doi:10.1021/acsnano.3c04175
55. Liu Y, Zhu X, Wei Z, et al. Multi-Channel Lanthanide Nanocomposites for Customized Synergistic Treatment of Orthotopic Multi-Tumor Cases. *Angew Chem Int Ed Engl*. 2023;62(30):e202303570. doi:10.1002/anie.202303570
56. Cui J, Zhang F, Yan D, et al. "Trojan Horse" Phototheranostics: fine-Engineering NIR-II AIEgen Camouflaged by Cancer Cell Membrane for Homologous-Targeting Multimodal Imaging-Guided Phototherapy. *Adv. Mater.* 2023;35(33). doi:10.1002/adma.202302639
57. Cheng J, Zhu Y, Dai Y, et al. Gas-Mediated Tumor Energy Remodeling for Sensitizing Mild Photothermal Therapy. *Angew Chem Int Ed Engl*. 2023;62(27):e202304312. doi:10.1002/anie.202304312
58. Yu Y, Tang D, Liu C, et al. Biodegradable Polymer with Effective Near-Infrared-II Absorption as a Photothermal Agent for Deep Tumor Therapy. *Adv Mater*. 2021;34(4):e2105976. doi:10.1002/adma.202105976
59. Zuo W, Liu N, Chang Z, et al. Single-site bimetallic nanosheet for imaging guided mutually-reinforced photothermal-chemodynamic therapy. *Chem Eng J*. 2022;442:136125. doi:10.1016/j.cej.2022.136125

60. Zhou G, Chen Y, Chen W, et al. Renal Clearable Catalytic 2D Au-Porphyrin Coordination Polymer Augmented Photothermal-Gas Synergistic Cancer Therapy. *Small*. 2023;19(14):e2206749. doi:10.1002/smll.202206749
61. Wang M, Chang M, Zheng P, et al. A Noble AuPtAg-GOx Nanozyme for Synergistic Tumor Immunotherapy Induced by Starvation Therapy-Augmented Mild Photothermal Therapy. *Adv Sci (Weinh)*. 2022;9(31):e2202332. doi:10.1002/advs.202202332